Supporting Information for

Cobalt nickel phosphide nanoparticles decorated carbon nanotubes as advanced hybrid catalyst for hydrogen evolution

Yuan Pan,[†] Yinjuan Chen,[†] Yan Lin,[†] Peixin Cui,[‡] Kaian Sun, Yunqi Liu,[*,†], Chenguang Liu[†]

[†]*State Key Laboratory of Heavy Oil Processing, Key Laboratory of Catalysis, China University of Petroleum (East China), Qingdao, 266580, P. R. China*

[‡]*National Synchrotron Radiation Laboratory, University of Science and Technology of China, Hefei, 230029, P. R. China*

[*]*Corresponding Authors: liuyq@upc.edu.cn;*

Experimental details

Materials

Nickel(II) acetylacetonate ($Ni(acac)_2$, 95%), cobalt(II) acetylacetonate ($Co(acac)_2$, 97%) trioctylphosphine (TOP, 90%), oleylamine (OAm, 95%), hydrazine hydrate (≥98%), and graphite powder (GP, 99.95%) and multiwall carbon nanotubes (CNTs, 95%, diam: 10-20 nm, length: 5-15 mm) were obtained from Aladdin Chemistry Co. Ltd. Hexane (≥99.5%), ethanol (≥99.7%), and sulfuric acid (H_2SO_4, 98%) were obtained from Sinopharm Chemical Reagent Co. Ltd. A Nafion solution (5% in a mixture of lower aliphatic alcohols and water) and Pt/C were purchased from Sigma-Aldrich. All chemicals were used as received without further purification.

Synthesis of pure Ni_2P catalyst

In a typical synthesis, $Ni(acac)_2$ (0.256 g, 1 mmol) and OAm (10 mL, 30.4 mmol) were placed in a four-neck flask and stirred magnetically under a flow of argon. The mixture was heated to 120 ^{o}C and kept at this temperature for 30 min. Then TOP (3.5 mL, 7.7 mmol) was injected into the solution, the mixture was rapidly heated to 320 ^{o}C and vigorously stirred for 2 h. After cooling to room temperature, the product was collected, centrifuged, washed with a mixture of hexane and ethanol, and finally dried in vacuum at 60 ^{o}C for 24 h.

Synthesis of pure CoP catalyst

In a typical synthesis, $Co(acac)_2$ (0.257 g, 1 mmol), ODE (5 mL, 15.6 mmol) and OAm (10 mL, 30.4 mmol) were placed in a four-neck flask under a flow of argon. The mixture was stirred and heated to 120 ^{o}C and kept at this temperature for 30 min. Then TOP (5 mL, 11 mmol) was added to the above solution and heated to 330 ^{o}C for 1 h. After cooling to room temperature, the product was collected, centrifuged, washed with a mixture of hexane and ethanol, and finally dried in

vacuum at 60 °C for 24 h.

Synthesis of $Co_{2-x}Ni_xP$/CNTs hybrid catalysts with different Co atoms

CNTs were treated with concentrated nitric acid according to a previous reported method [1]. The $Co_{2-x}Ni_xP$/CNTs hybrid catalysts were synthesized as follows: In a typical synthesis, $Ni(acac)_2$ (0.096 g, 0.375 mmol), $Co(acac)_2$ (0.032 g, 0.125 mmol), OAm (7 mL, 21.3 mmol) and CNTs (after acid treatment, 50 mg) were placed in a four-neck flask and stirred magnetically under a flow of argon. The mixture was heated to 120 °C and kept at this temperature for 30 min. Then TOP (3.4 mL, 7.5 mmol) was injected into the solution, the mixture was rapidly heated to 320 °C and vigorously stirred for 2 h. After cooling to room temperature, the product was collected, centrifuged, washed with a mixture of hexane and ethanol, and finally dried in vacuum at 60 °C for 24 h to get the $Co_{0.5}Ni_{1.5}P$/CNTs hybrid catalyst. Without changing the synthetic conditions, $Co_{1.1}Ni_{0.9}P$/CNTs and $Co_{1.6}Ni_{0.4}P$/CNTs were obtained by changing the molar ratio of Co: Ni precursor to 1.22 and 3, respectively. The $Co_{2-x}Ni_xP$ NPs were synthesized using the similar synthesis process except for without the addition of CNTs. *Note: the atomic molar ratio of Co: Ni: P of the as-synthesized $Co_{2-x}Ni_xP$/CNTs hybrid catalysts were confirmed from the XPS fitting results.*

Synthesis of $Co_{1.6}Ni_{0.4}P$/CNTs hybrid catalyst with different CNTs content

The synthesis of the $Co_{1.6}Ni_{0.4}P$/CNTs hybrid catalyst with different CNTs content (0, 10 mg, 20 mg) was similar to that of $Co_{1.6}Ni_{0.4}P$/CNTs-50, except for that the content of the CNTs was changed from 0 to 20 mg. In a typical synthesis, $Ni(acac)_2$ (0.0321 g, 0.125 mmol), $Co(acac)_2$ (0.0964 g, 0.375 mmol), OAm (7 mL, 21.3 mmol), and CNTs (after acid treatment, 0, 10, 20 mg) were placed in a four-neck flask and stirred magnetically under a flow of argon. Similarly, the

mixture was heated to 120 ^{o}C and kept at this temperature for 30 min. Then TOP (3.4 mL, 7.5 mmol) was injected into the solution, the mixture was rapidly heated to 320 ^{o}C and vigorously stirred for 2 h. After cooling to room temperature, the product was collected, centrifuged, and washed with a mixture of hexane and ethanol. Finally, the products were dried in vacuum at 60 ^{o}C for 24 h to obtain $Co_{1.6}Ni_{0.4}P$/CNTs-x (x=0, 10, 20) hybrid catalysts.

Materials characterizations

X-ray diffraction (XRD) was performed on a panalytical X'pert PROX-ray diffractometer with Cu Kα monochromatized radiation (λ= 1.54 Å) and operated at 45 kV and 40 mA. Transmission electron microscopy (TEM) was performed on a JEM-2100 UHR microscope (JEOL, Japan) at an accelerating voltage of 200 kV. Scanning electron microscope (SEM) images were obtained with a Hitachi S-4800 instrument at 5 kV. An energy dispersive X-ray (EDX) instrument was attached to the SEM and TEM systems. X-ray photoelectron spectroscopy (XPS) was performed on a VG ESCALABMK II spectrometer using an Al Kα (1486.6 eV) photon source. N_2 adsorption-desorption experiments were carried out on a ChemBET 3000 (Quantachrome, USA) instrument. Inductively coupled plasma-optical emission spectrometry (ICP-OES) analysis was performed on a Thermo iCAP 6300 instrument. X-ray absorption fine structure (XAFS) were carried out in transmission mode with a Si (111) monochromator on Beamline 20-BM at Advanced Photon Source (APS), Argonne National Laboratory. The typical energy of the storage ring was 7 GeV in and experiments were performed with 100 mA in top-up progress. The incident beam intensity was monitored using an ionization chamber flowed by nitrogen while the transmission signal was collected by another ionization chamber flowed by argon.

Electrochemical measurements

The HER catalytic activity measurement of the as-synthesized $Co_{2-x}Ni_xP$/CNTs hybrid catalysts was performed in a standard three-electrode system controlled by a Reference 600 instrument (Gamry Instruments, USA). A Ag/AgCl electrode was used as reference electrode and a Pt electrode as counter electrode. Linear sweep voltammetry (LSV) was carried out at 5 $mV \cdot s^{-1}$ for the polarization curves in 0.5 M H_2SO_4 solutions. All the polarization curves were iR-corrected. The double layer capacitance (C_{dl}) was conducted with cyclic voltammograms (CVs) scanning from 0.1 to 0.2 V vs. RHE with different scan rates from 40 to 300 $mV \cdot s^{-1}$. The durability test was carried out by CVs scanning 500 cycles with a scan rate of 100 $mV \cdot s^{-1}$ in 0.5 M H_2SO_4. Electrochemical impedance spectroscopy (EIS) measurements were carried out in 0.5 M H_2SO_4 at various overpotentials from 60 to 140 mV (vs. reversible hydrogen electrode (RHE)) in the frequency range of 100 kHz to 0.1 Hz with a single modulated AC potential of 5 mV. The experimental EIS data were analyzed and fitted with the software of Zsimpwin. All the potentials reported in our work are versus the RHE, namely E (RHE) = E (Ag/AgCl) + (0.222 + 0.059 pH).

Preparation of working electrodes

To prepare the $Co_{2-x}Ni_xP$/CNTs hybrids on glassy carbon electrode (GCE, 4 mm in diameter), 5 mg of hybrid and 80 μL Nafion solution (5 wt. %) were dispersed in 1 mL ethanol and sonicated for 30 min to form a slurry. Subsequently, 5 μL of suspension was dropped on GCE and the electrode was dried at room temperature.

Calculation of the number of active sites and turnover frequency (TOF)

The number of active sites (n) was determined using a previously reported method [2] by CV collected from -0.2 to +0.6 V vs. RHE in 1.0 M phosphate buffer solution (PBS, pH = 7) with a scan rate of 20 $mV \cdot s^{-1}$. While it is difficult to assign the observed peaks to a given redox couple, n

should be proportional to the integrated charge over the whole potential range. Assuming a one-electron process for both reduction and oxidation, the upper limit of n could be calculated with the equation:

$$n = \frac{\mathbf{Q}}{2\mathbf{F}}$$

TOF can be calculated with the equation:

$$TOF = \frac{I}{2Fn}$$

where Q is the voltammetric charge, F is the Faraday constant (96485 $C \cdot mol^{-1}$), I is the current (A) during the linear sweep measurement and n is the numbers of active sites (mol). The factor 1/2 in equation represents two electrons are required to form one hydrogen molecule from two protons.

Computational method

The density functional theory (DFT) based calculations presented in this work were carried out with the Dmol3 module in the Materials Studio package from Accelrys (version 8.0) [3]. The double numerical plus polarization (DNP) basis set with OBS [4] parameters for the van der Waals dispersion correction and PW91 exchange-correlation functional were used. Semi-core pseudopotentials (DSPPs) [5] were used to treat the core electrons of nickel and cobalt.

The Ni_2P unit cell was fully optimized with all the atoms relaxed. The $Co_{1.5}Ni_{0.5}P$ unit cell was build on the basic of a geometry optimized Ni_2P unit cell by changing the population of cobalt and nickel on the primary nickel sites to 75 percent and 25 percent, respectively. A 5-layer slab with 46 original atoms was cleaved for the surface catalytic performance study.

To orientate the transition state geometries, the traditional linear and quadratic synchronous transient (LST/QST) methods [6] were further confirmed by minimum-energy pathway (MEP)

calculation using the nudge elastic band (NEB) [7] method. Considering the excellent migratory aptitude of single hydrogen atom, two different assembles of H atomic adsorption were chosen as displayed in Fig. S13. (a) and (b).

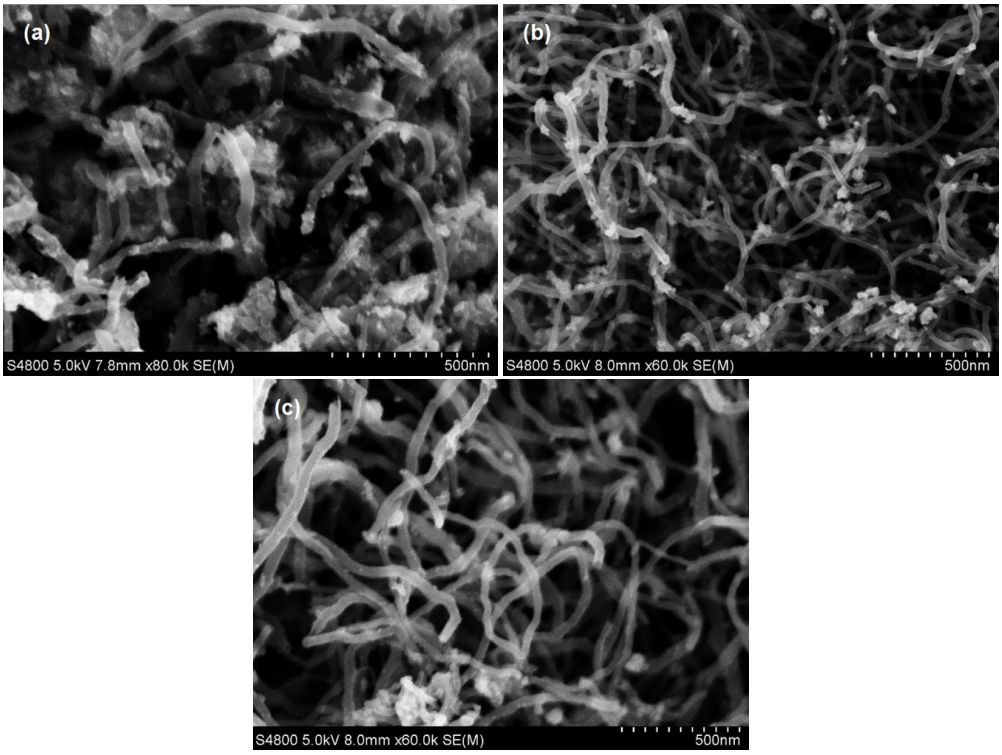

Fig. S1 SEM images of (a) $Co_{0.5}Ni_{1.5}P$/CNTs, (b) $Co_{1.1}Ni_{0.9}P$/CNTs and (c) $Co_{1.6}Ni_{0.4}P$/CNTs hybrid catalysts.

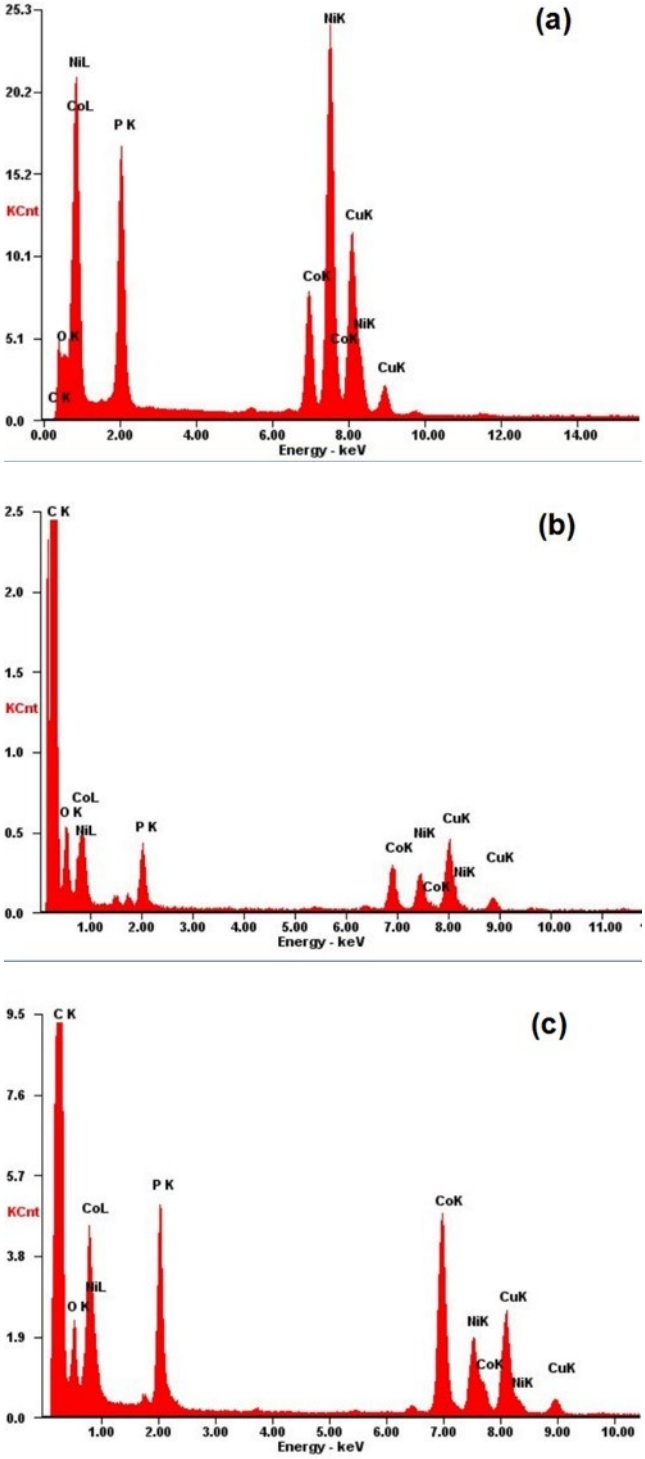

Fig. S2 EDX spectra of (a) $Co_{0.5}Ni_{1.5}P$/CNTs, (b) $Co_{1.1}Ni_{0.9}P$/CNTs and (c) $Co_{1.6}Ni_{0.4}P$/CNTs hybrid catalysts.

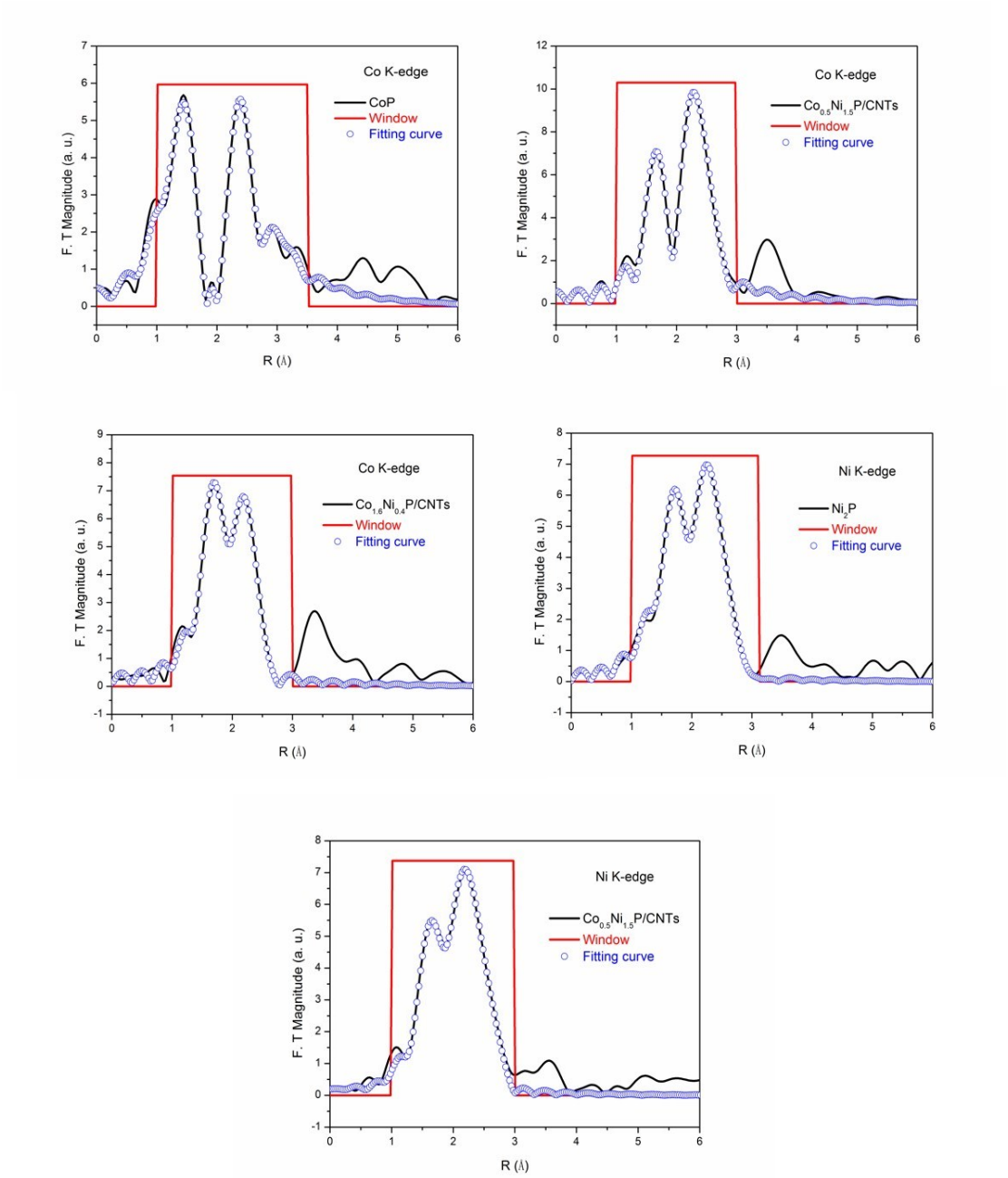

Fig. S3 FT-EXAFS spectra at the Co K-edge of CoP, $Co_{0.5}Ni_{1.5}P$/CNTs and $Co_{1.6}Ni_{0.4}P$/CNTs and their fitting curves. FT-EXAFS spectra at the Ni K-edge of Ni_2P and $Co_{0.5}Ni_{1.5}P$/CNTs and their fitting curves.

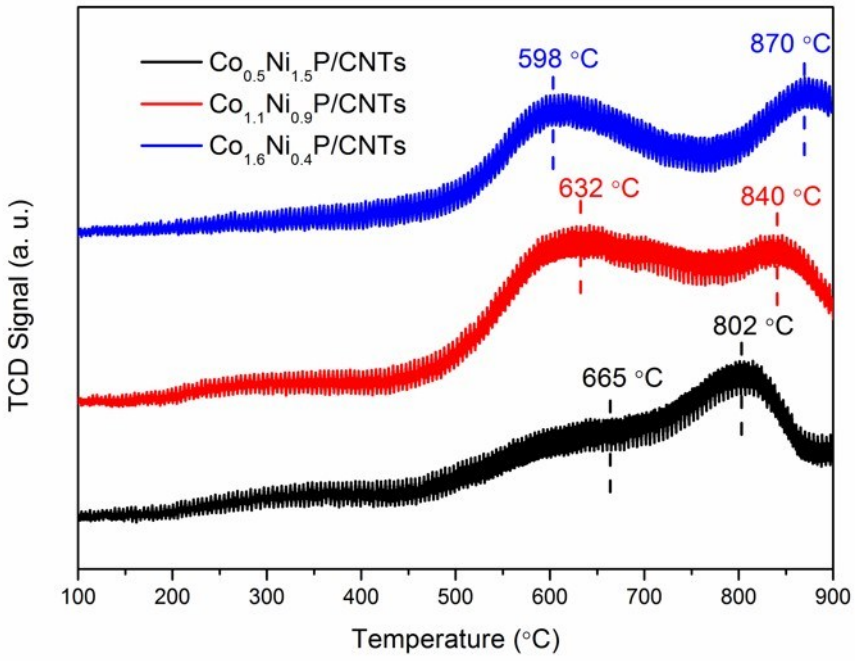

Fig. S4 H_2-TPD spectra for the as-synthesized $Co_{2-x}Ni_xP$/CNTs hybrid catalysts.

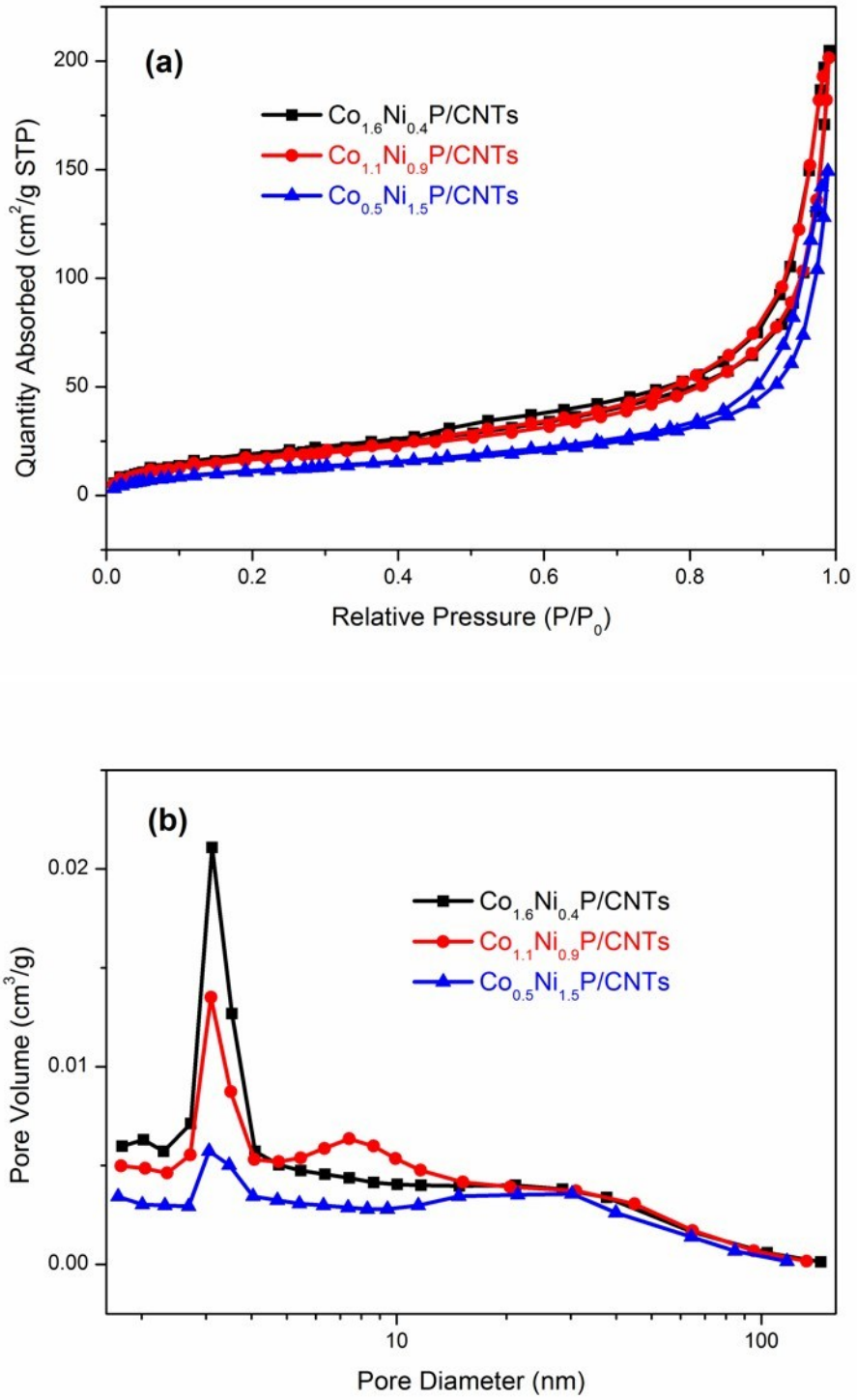

Fig. S5 (a) Nitrogen sorption isotherms and (b) BJH pore-size distribution curves of the as-synthesized $Co_{2-x}Ni_xP$/CNTs hybrid catalysts.

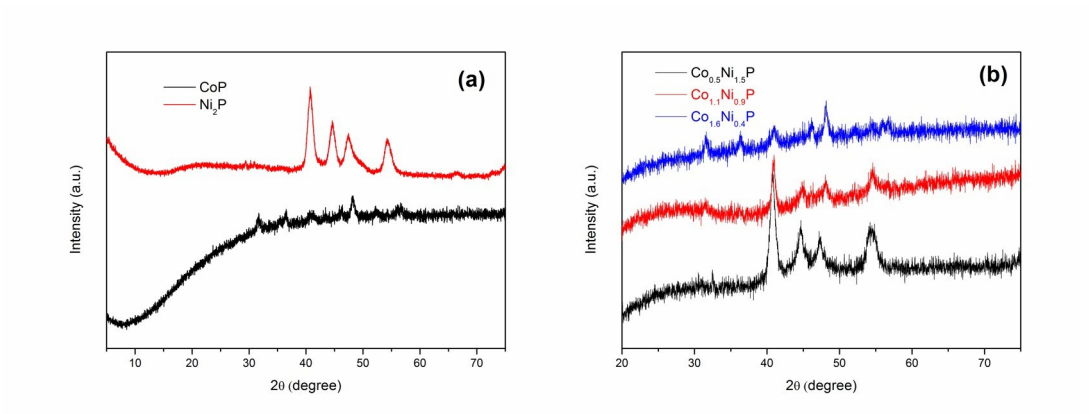

Fig. S6 XRD patterns of the as-synthesized (a) Ni_2P and CoP, (b) $Co_{2-x}Ni_xP$ NPs.

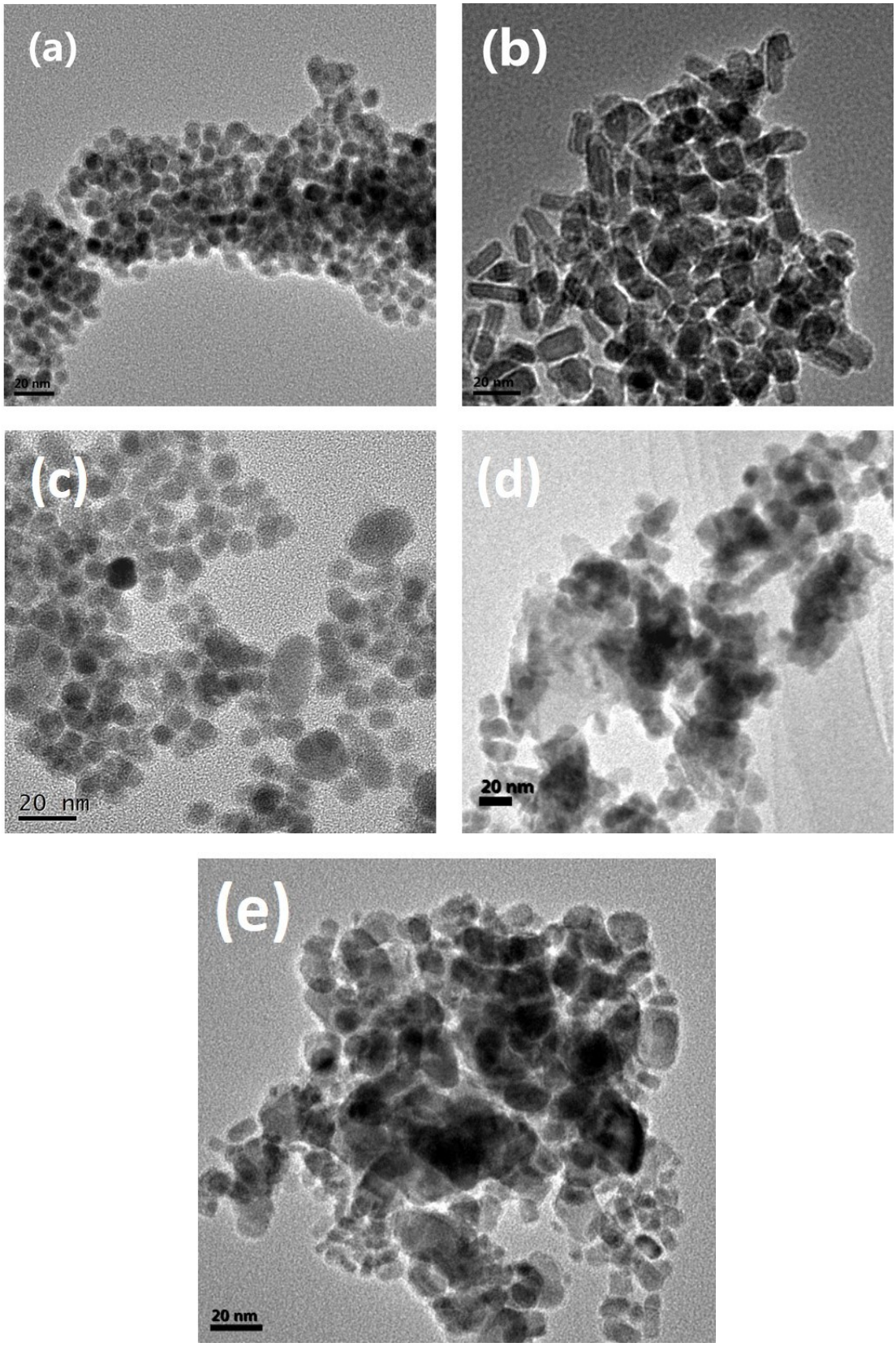

Fig. S7 TEM images of the as-synthesized (a) Ni_2P, (b) CoP, (c) $Co_{0.5}Ni_{1.5}P$, (d) $Co_{1.1}Ni_{0.9}P$ and (e) $Co_{1.6}Ni_{0.4}P$ NPs.

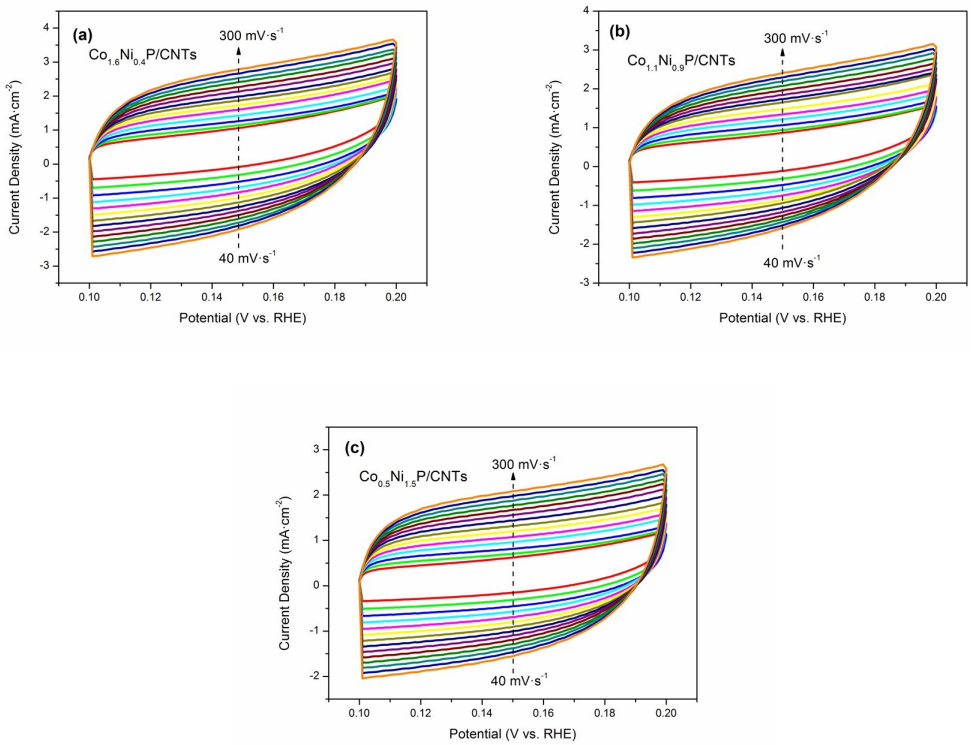

Fig. S8 CVs of the as-synthesized $Co_{2-x}Ni_xP$/CNTs hybrid catalysts in 0.5 M H_2SO_4 solution in the region of 0.1-0.2 V vs. RHE with different scan rates from 40 mV·s-1 to 300 mV·s^{-1}.

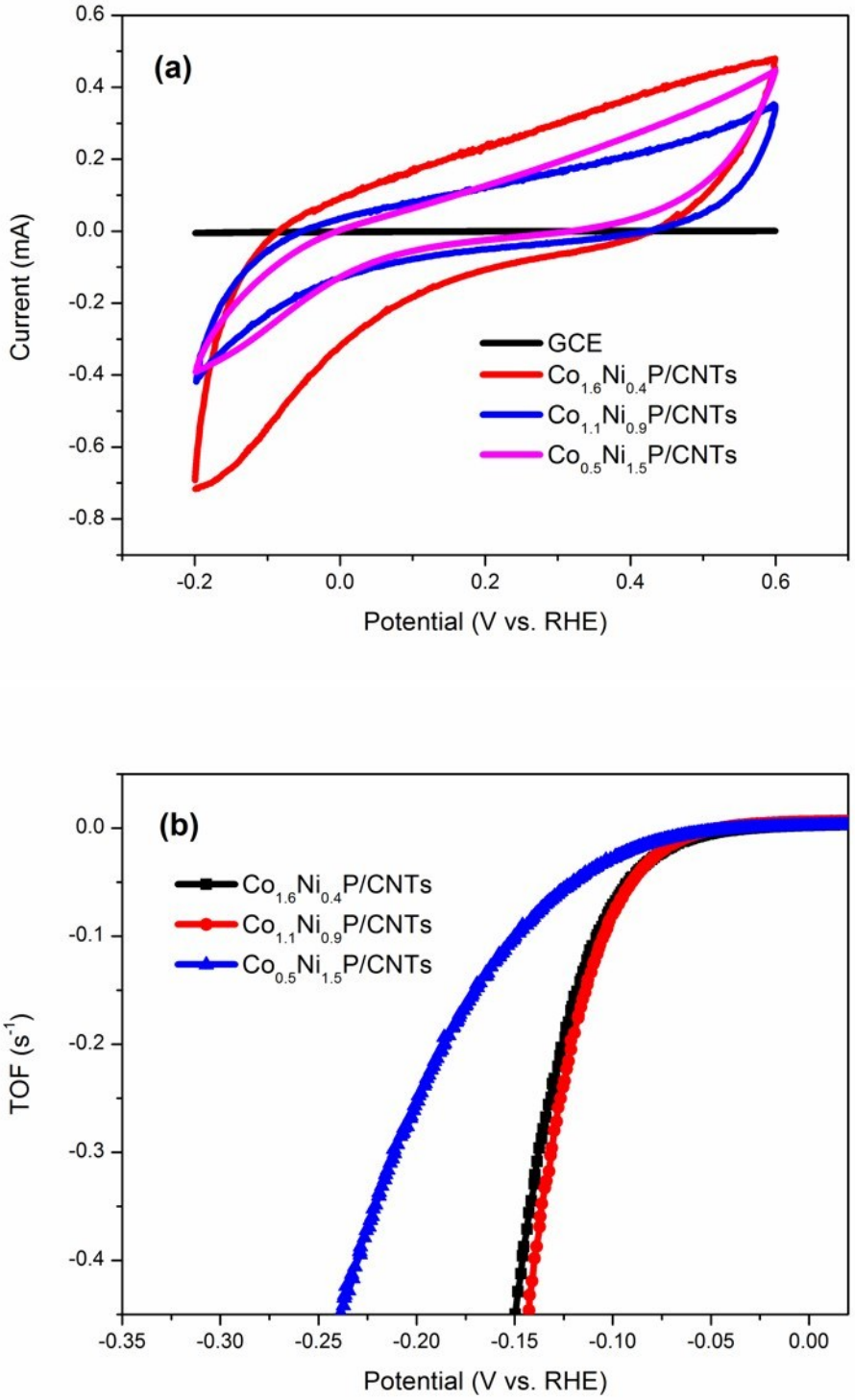

Fig. S9 (a) CVs of the $Co_{2-x}Ni_xP$/CNTs hybrid catalysts recorded in PBS electrolyte (pH = 7) with a scan rate of 20 mV·s^{-1}. (b) LSV polarization curves of the as-synthesized $Co_{2-x}Ni_xP$/CNTs hybrid catalysts normalized by the active sites and expressed in terms of TOF.

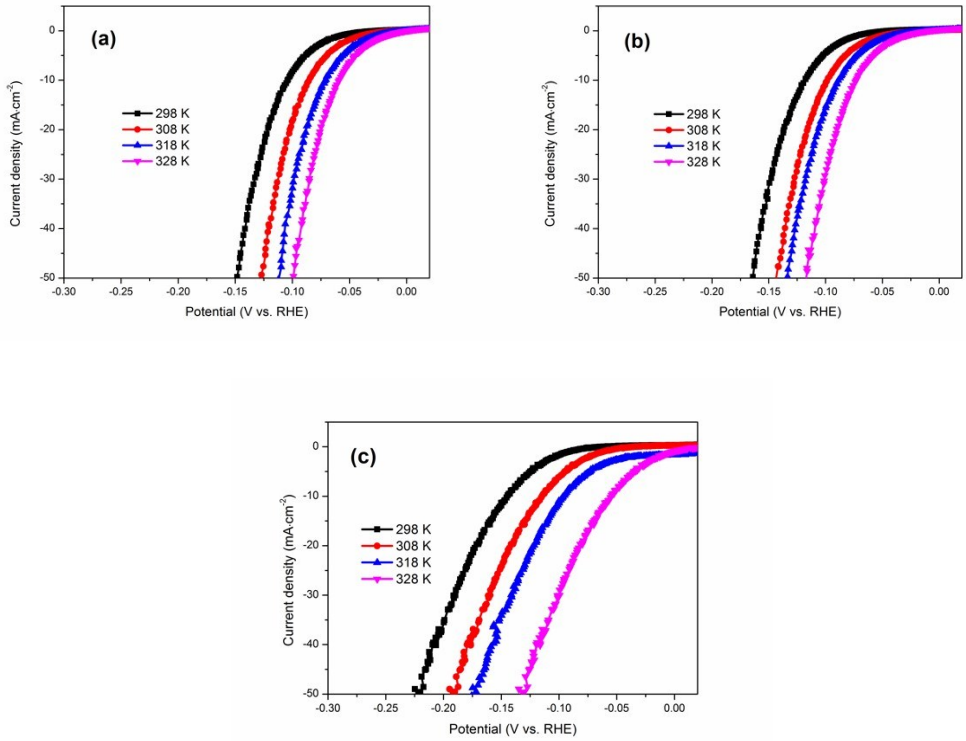

Fig. S10 LSV polarization curves of the (a) $Co_{1.6}Ni_{0.4}P$/CNTs, (b) $Co_{1.1}Ni_{0.9}P$/CNTs and (c) $Co_{0.5}Ni_{1.5}P$/CNTs hybrid catalysts at different temperature.

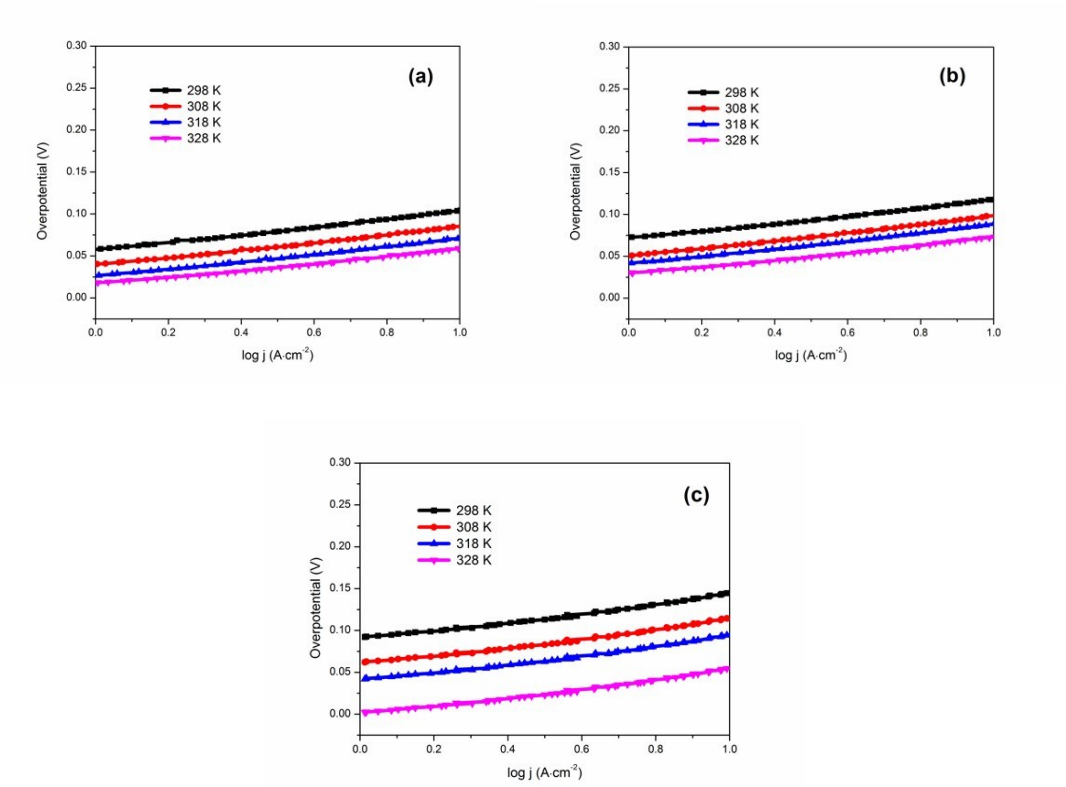

Fig. S11 Tafel plots of the (a) $Co_{1.6}Ni_{0.4}P$/CNTs, (b) $Co_{1.1}Ni_{0.9}P$/CNTs and (c) $Co_{0.5}Ni_{1.5}P$/CNTs hybrid catalysts at different temperature.

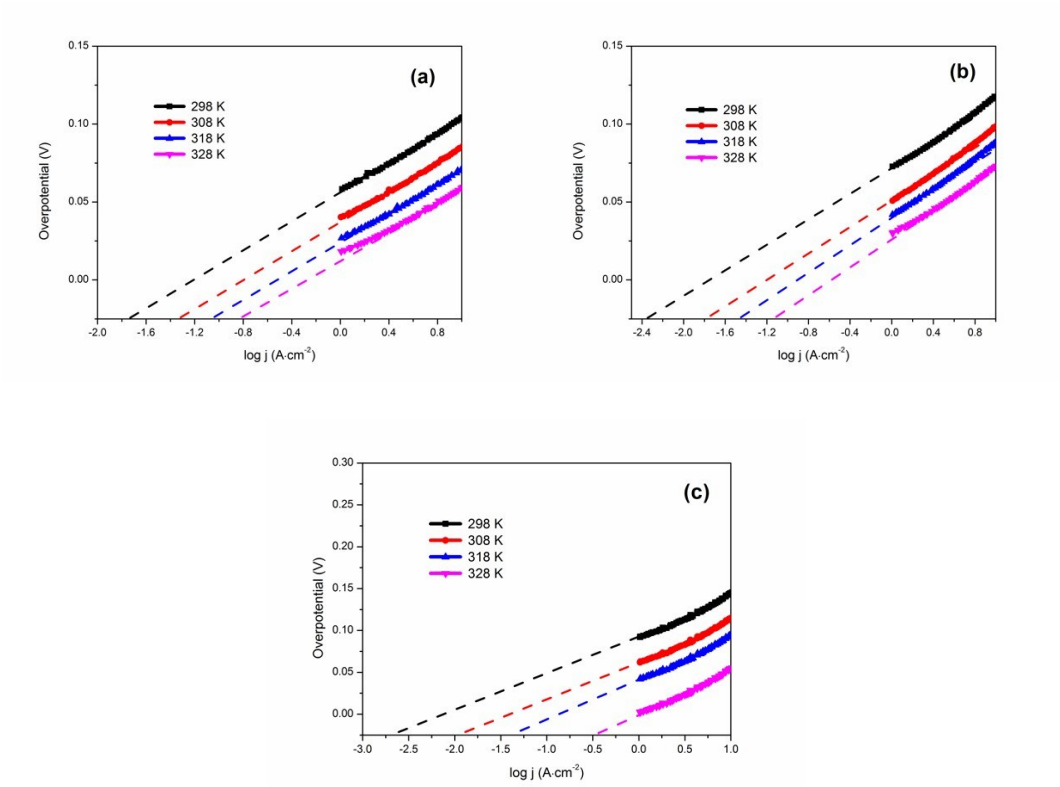

Fig. S12 Exchange current densities of the (a) $Co_{1.6}Ni_{0.4}P$/CNTs, (b) $Co_{1.1}Ni_{0.9}P$/CNTs and (c) $Co_{0.5}Ni_{1.5}P$/CNTs hybrid catalysts at different temperature.

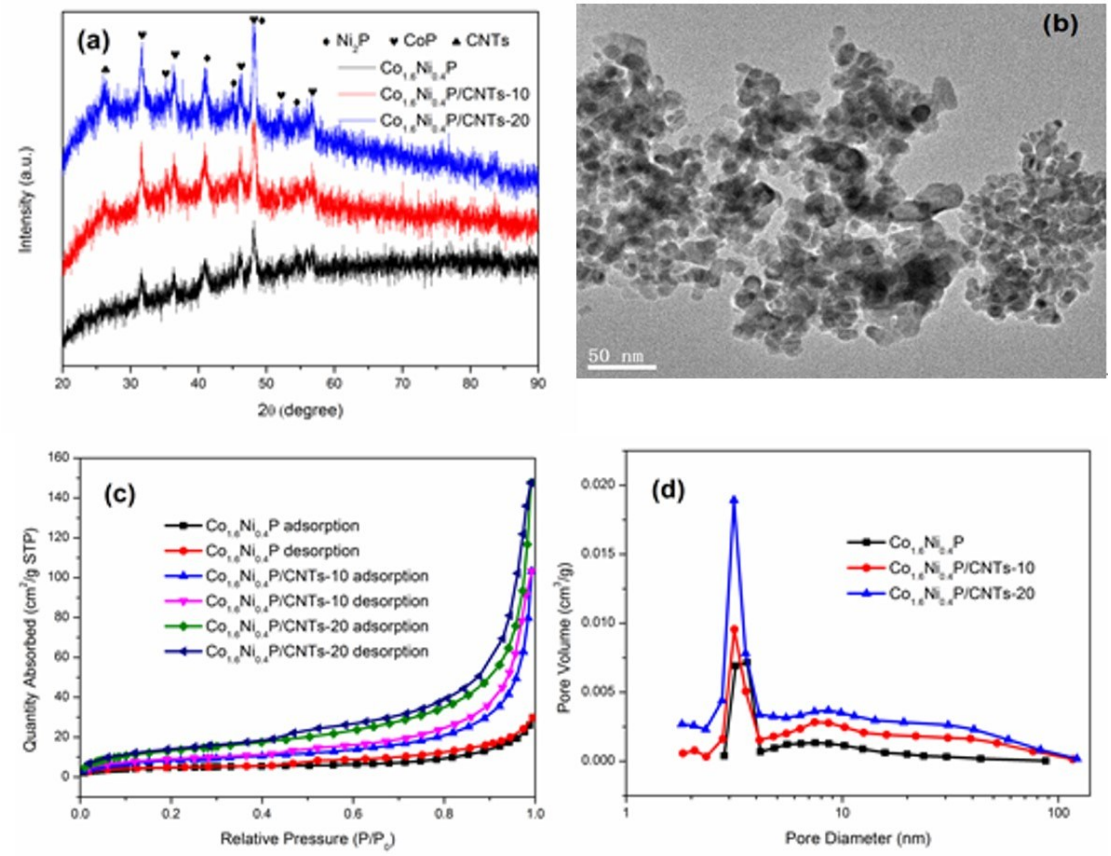

Fig. S13 (a) XRD patterns of the as-synthesized $Co_{1.6}Ni_{0.4}P$/CNTs hybrid catalysts with different carbon content. (b) TEM image of $Co_{1.6}Ni_{0.4}P$ nanoparticles. (c) Nitrogen sorption isotherms and (d) BJH pore-size distribution curve of the as-synthesized $Co_{1.6}Ni_{0.4}P$/CNTs hybrid catalysts with different carbon content.

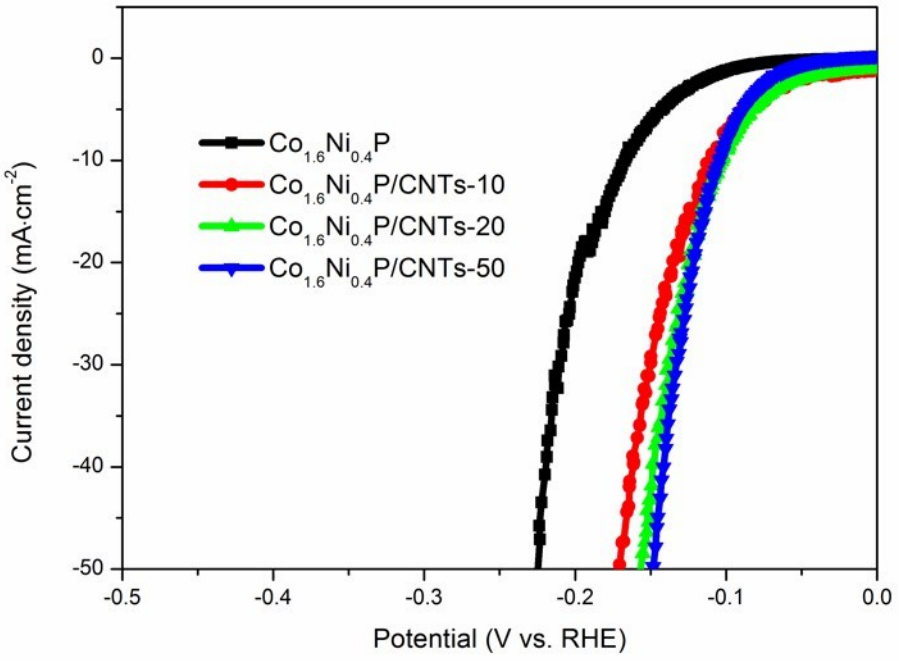

Fig. S14 LSV curves of $Co_{1.6}Ni_{0.4}P$/CNTs hybrid catalyst with different carbon content.

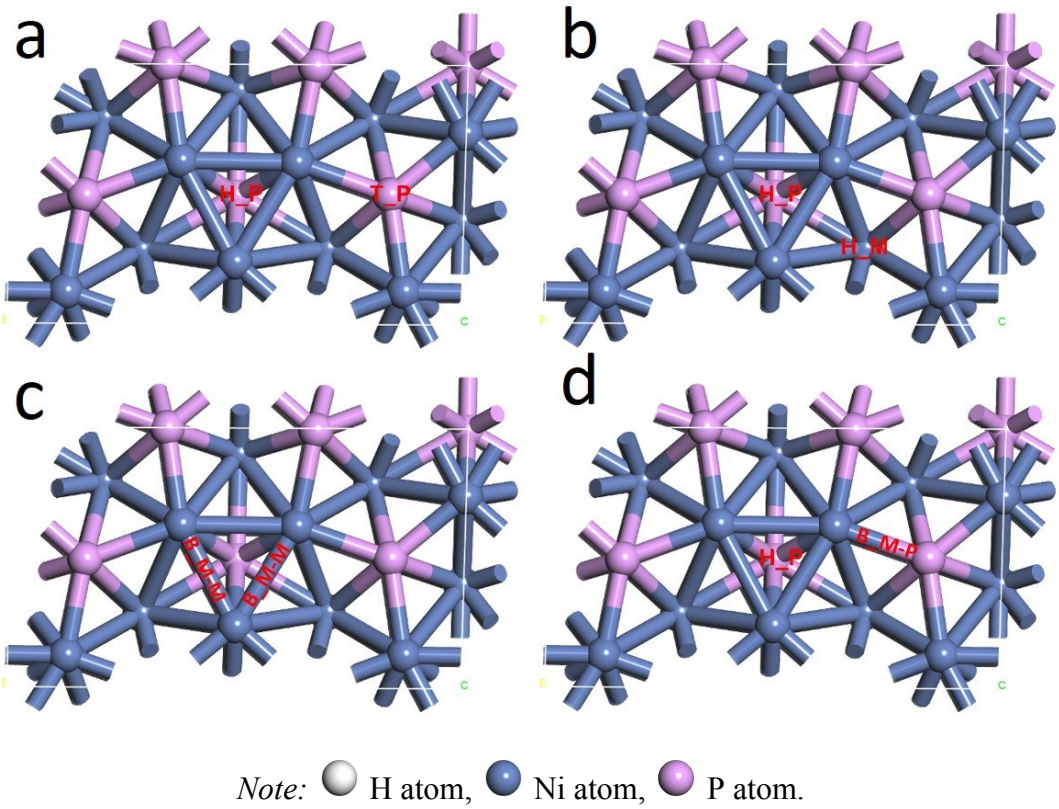

Note: H atom, Ni atom, P atom.

Fig. S15 Primarily chose H atom adsorption site. (a) The center hollow site of three Ni or Co atoms and the top site of a P atom are presented with H_P and T_P in the graph. (b) The center hollow site of three metal atoms assembled with the center hollow site of three metal atoms and two P atoms, which presented with H_P and H_M in the graph. (c) and (d) are optimized H atomic adsorption sites for Ni_2P according to the geometry optimized $Co_{1.5}Ni_{0.5}P$ adsorption configuration (a) and (b) respectively, which set the H atom at two Ni-Ni bridge sites (B_M-M) and the center hollow site of three Ni atoms (H_P) associated with the Ni-P bridge site (B_M-P).

Table S1 ICP-OES analysis results of the as-synthesized $Co_{2-x}Ni_xP$/CNTs.

Catalyst	Co (ω %)	Ni (ω %)	P (ω %)
$Co_{0.5}Ni_{1.5}P$/CNTs	6.68	24.03	7.97
$Co_{1.1}Ni_{0.9}P$/CNTs	15.99	18.15	9.38
$Co_{1.6}Ni_{0.4}P$/CNTs	24.27	7.89	9.41

Table S2 Values of the absorption edge position for Ni K-edge and Co K-edge.

Ni K-edge	Absorption edge position (eV)
Ni-foil	8333.3
NiO	8344.3
Ni_2P	8337.6
Ni_2P/CNTs	8337.6
$Co_{0.5}Ni_{1.5}P$/CNTs	8337.6
$Co_{1.6}Ni_{0.4}P$/CNTs	8338.5

Co K-edge	Absorption edge position (eV)
Co-foil	7709.9
CoO	7722.4
Co_3O_4	7728.4
CoP	7723.5
$Co_{0.5}Ni_{1.5}P$/CNTs	7715.8
$Co_{1.6}Ni_{0.4}P$/CNTs	7716.7

Table S3 EXAFS fitting parameters at the Ni K-edge and Co K-edge of Ni_2P/CNTs, $Co_{0.5}Ni_{1.5}P$/CNTs, $Co_{1.6}Ni_{0.4}P$/CNTs and CoP catalysts[a].

Catalyst	Shell	N	R_j (Å)	$\sigma^2(\times10^{-3})$ (Å^2)	ΔE_0 (eV)
Ni_2P/CNTs	Ni-P	5	2.22	2.7	-15
	Ni-Ni	6	2.67	3.7	2.8
	Ni-Ni	6	2.96	2.1	2.8
$Co_{0.5}Ni_{1.5}P$/CNTs	Ni-P	5	2.26	7.4	-5.5
	Co-Ni	4.2	2.66	4.3	6.7
	Co-P	5.1	2.30	9.6	3.2
$Co_{1.6}Ni_{0.4}P$/CNTs	Co-Ni(Co)	8.0	2.55	12	-9.1
	Co-P	3.6	2.24	6.2	-4.7
CoP	Co-Co	8	2.81	40	-40
	Co-Co	12	3.13	9.5	-40
	Co-P	6	2.02	15	-38
	Co-P	8	3.14	1.2	-38

[a]N, coordination number; R_j, bonding distance; σ^2, Debye-Waller factor; ΔE_0, inner potential shift.

Table S4 Textural properties of the as-synthesized $Co_{2-x}Ni_xP$/CNTs hybrid catalysts.

Catalyst	BET surface area ($m^2 \cdot g^{-1}$)	Pore volume ($cm^3 \cdot g^{-1}$)	Pore size (nm)
$Co_{1.6}Ni_{0.4}P$/CNTs	68.8	0.31	14.9
$Co_{1.1}Ni_{0.9}P$/CNTs	64.3	0.3	15.5
$Co_{0.5}Ni_{1.5}P$/CNTs	43.1	0.22	17.5
$Co_{1.6}Ni_{0.4}P$	17.3	0.04	11.1
$Co_{1.6}Ni_{0.4}P$/CNTs-10	31.1	0.15	18.7
$Co_{1.6}Ni_{0.4}P$/CNTs-20	49.2	0.22	15.7

Table S5 Comparison of the HER catalytic performance of some reported HER catalysts in 0.5 M H_2SO_4.

Catalyst	Current density ($mA \cdot cm^{-2}$)	Potential (mV)	$J_{exchange}$ ($mA \cdot cm^{-2}$)	Tafel slope ($mV \cdot dec^{-1}$)	Reference
β-INS nanosheets	10	117	0.014	48	8
α-INS nanosheets	10	105	0.02	40	8
$Fe_{0.9}Co_{0.1}S_2$/CNT	20	120	--	46	9
CoS_2@MoS_2	10	110.5	--	57.3	10
α-WNP	20	110	0.044	39	11
$Fe_{0.48}Co_{0.52}S_2$	10	196	--	47.5	12
$Co_{1.33}Ni_{0.67}P$/Ti	20	430	0.071	161	13
$Co_{1.33}Ni_{0.67}P$/GCE	20	240	0.0059	57	13
$Co_{0.59}Fe_{0.41}P$	10	72	0.517	52	14
NiWS	8.6	250	---	55	15
Cu-MoS_2/rGO	81.6	400	0.0776	90	16
$Co_{0.5}Ni_{1.5}P$/CNTs	20	169.8	0.0024	60.9	This work
$Co_{1.1}Ni_{0.9}P$/CNTs	20	135.4	0.0046	53.1	This work
$Co_{1.6}Ni_{0.4}P$/CNTs	20	118.8	0.0186	46.7	This work

Table S6 Values of elements in equivalent circuit resulted from fitting the EIS data.

Potential (mV) vs. RHE	R_s (Ω)	Q ($F \cdot cm^{-2} \cdot S^{n-1}$)	n	R_{ct} (Ω)
-60	7.926	0.002422	0.8	517
-80	8.133	0.002924	0.8	210.8
-100	7.443	0.00327	0.8	90.17
-120	7.494	0.003391	0.8	43.08
-140	7.497	0.003067	0.8	23.74

Table S7 Kinetic parameters of the as-synthesized $Co_{2-x}Ni_xP$/CNTs hybrid catalysts.

Catalyst	T (K)	Tafel ($mV \cdot dec^{-1}$)	J_0 ($A \cdot cm^{-2}$)	E_a ($kJ \cdot mol^{-1}$)
$Co_{1.6}Ni_{0.4}P$/CNTs	298	46.7	1.86×10^{-5}	57.3
	308	42.9	4.79×10^{-5}	
	318	39	9.33×10^{-5}	
	328	36.3	1.55×10^{-4}	
$Co_{1.1}Ni_{0.9}P$/CNTs	298	53.1	4.57×10^{-6}	75.2
	308	46.2	1.69×10^{-5}	
	318	44.1	3.55×10^{-5}	
	328	40	7.76×10^{-5}	
$Co_{0.5}Ni_{1.5}P$/CNTs	298	60.9	2.39×10^{-6}	132.9
	308	55.7	1.23×10^{-5}	
	318	51.4	4.68×10^{-5}	
	328	45.6	3.63×10^{-4}	

References

[1] T. W. Lin, C. G. Salzmann, L. D. Shao, C. H. Yu, M. L. H. Green, S. C. Tsang, Carbon, 2009, 47, 1415.

[2] (a) H. Du, Q. Liu, N. Cheng, A. M. Asiri, X. Sun, C. M. Li, J. Mater. Chem. A, 2014, 2, 14812. (b) P. Jiang, Q. Liu, X. Sun, Nanoscale, 2014, 6, 13440. (c) Z. Pu, Q. Liu, C. Tang, A. M. Asiri, X. Sun, Nanoscale, 2014, 6, 11031.

[3] (a) P. Hohenberg, W. Kohn, Phys. Rev. B, 1964, 136, 864. (b) M. Levy, Proc. Natl. Acad. Sci. U. S. A. 1979, 76, 6062.

[4] F. Ortmann, F. Bechstedt, W. G. Schmidt, Phys. Rev. B, 2006, 73, 205101.

[5] B. Delley, J. Phys.: Condens. Matter, 2010, 22, 384208.

[6] T. A. Halgren, W. N. Lipscomb, Chem. Phys. Lett., 1977, 49, 225.

[7] G. Henkelman, H. Jonsson, J. Chem. Phys. 2000, 113, 9978.

[8] X. Long, G. X. Li, Z. L. Wang, H. Y. Zhu, T. Zhang, S. Xiao, W. Y. Guo, S. H. Yang, J. Am. Chem. Soc., 2015, 137, 11900.

[9] D. Y. Wang, M. Gong, H. L. Chou, C. J. Pan, H. A. Chen, Y. Wu, M. C. Lin, M. Guan, J. Yang, C. W. Chen, Y. L. Wang, B. J. Hwang, C. C. Chen, H. J. Dai, J. Am. Chem. Soc., 2015, 137, 1587.

[10] H. C. Zhang, Y. J. Li, T. H. Xu, J. B. Wang, Z. Y. Huo, P. B. Wan, X. M. Sun, J. Mater. Chem. A, 2015, 3, 15020.

[11] Z. Y. Jin, P. P. Li, X. Huang, G. F. Zeng, Y. Jin, B. Z. Zheng, D. Xiao, J. Mater. Chem. A, 2014, 2, 18593.

[12] M. S. Faber, M. A. Lukowski, Q. Ding, N. S. Kaiser, S. Jin, J. Phys. Chem. C, 2014, 118,

21347.

[13] A. L. Lu, Y. Z. Chen, H. Y. Li, A. Dowd, M. B. Cortie, Q. S. Xie, H. Z. Guo, Q. Q. Qi, D. L. Peng, Int. J. Hydrogen Energ., 2014, 39, 18919.

[14] J. H. Hao, W. S. Yang, Z. Zhang, J. L. Tang, Nanoscale, 2015, 7, 11055.

[15] L. Yang, X. L. Wu, X. S. Zhu, C. Y. He, M. Meng, Z. X. Gan, P. K. Chu, Appl. Surf. Sci., 2015, 341, 149.

[16] F. Li, L. Zhang, J. Li, X. Q. Lin, X. Z. Li, Y. Y. Fang, J. W. Huang, W. Z. Li, M. Tian, J. Jin, R. Li, J. Power Sources, 2015, 292, 15.